

An *Ab initio* Force Field for the Cofactors of Bacterial Photosynthesis

MATTEO CECCARELLI,^{1,*} PIERO PROCACCI,² MASSIMO MARCHI³

¹CECAM, Centre Européen de Calcul Atomique et Moléculaire, Ecole Normale Supérieure de Lyon, 46 Allée d'Italie, 69364 Lyon, France

²Laboratorio di Spettroscopia Molecolare, Dipartimento di Chimica, Università degli Studi di Firenze, 50121 Firenze, Italy

³Commissariat à l'Énergie Atomique, DSV-DBCM-SBPM, Centre d'Études, Saclay, 91191 Gif-sur-Yvette Cedex, France

Received 13 February 2002; Accepted 13 February 2002

Abstract: This article presents a new *ab initio* force field for the cofactors of bacterial photosynthesis, namely quinones and bacteriochlorophylls. The parameters have been designed to be suitable for molecular dynamics simulations of photosynthetic proteins by being compatible with the AMBER force field. To our knowledge, this is the first force field for photosynthetic cofactors based on a reliable set of *ab initio* density functional reference data for methyl bacteriochlorophyll *a*, methyl bacteriopheophytin *a*, and of a derivative of ubiquinone. Indeed, the new molecular mechanics force field is able to reproduce very well not only the experimental and *ab initio* structural properties and the vibrational spectra of the molecules, but also the eigenvectors of the molecular normal modes. For this reason it might also be helpful to understand vibrational spectroscopy results obtained on reaction center proteins.

© 2002 Wiley Periodicals, Inc. J Comput Chem 24: 129–142, 2003

Key words: *ab initio* force field; bacterial photosynthesis

Introduction

Chlorophylls and quinones play a fundamental role in plants and bacterial photosynthesis. The former are found in reaction center (RC) and light harvesting proteins involved in the primary charge separation and in the collection of light, respectively. Quinones also bind to RCs, but are involved in the proton transfer from one side to the other of the cellular membrane. Both electronic and vibrational spectroscopies of these cofactors are crucial to the investigation of the structure and dynamics of reaction centers. Indeed, because of their characteristic electronic spectra, chlorophylls have been used in resonant Raman (RR) and Fourier transform infrared (FTIR) experiments on photosynthetic proteins as selective probes of the structural transformations occurring upon site-directed mutagenesis on the underlying protein. FTIR spectroscopy is also used to evince the proton transfer path in reaction centers from changes in hydrogen bonding structure of the environment around the quinones. More recently, μs time resolution has been obtained in time-resolved FTIR investigation of electron transfer between quinones Q_A and Q_B in the bacterial reaction center of *Rhodobacter (Rb) sphaeroides*. Finally, femtosecond kinetics of electron transfer and excitation relevant to photosynthesis are routinely explored by time resolved electronic tech-

niques, such as stimulated emission and absorption. In many instances, coupling between electronic and nuclear coordinates of the cofactors affects in a nontrivial way the results of these experiments.

This large amount of spectroscopic data has elicited theoretical work on the assignment of the vibrational spectra of these cofactors. In the past, empirical and semiempirical approaches have been used to obtain a normal mode description of chlorophylls and quinones.^{1–3} These techniques, although undemanding computationally, have the key most disadvantage that they are dependent on a set of free parameters, which in turn, are determined based, usually, on results on model compounds and on the chemical sense of the investigators. *Ab initio* methods based on the density func-

*Present address: CSCS/ETHZ, Via Cantonale, CH-6928 Manno, Switzerland; e-mail: mcecca@cscs.ch

Correspondence to: M. Marchi; e-mail: marchi@villon.saclay.cea.fr

Contract/grant sponsor: European Union grant Marie Curie Fellowship; contract/grant number: ERBFMBICT983308 (to M.C.)

This article includes Supplementary Material available from the authors upon request or via the Internet at <ftp://ftp.wiley.com/public/journals/jcc/suppmat/24/129> or <http://www.interscience.wiley.com/jpages/0192-8651/suppmat/v24.129.html>

tional theory (DFT) have only began to be applied to these cofactors in recent times.^{4–6} Unlike semiempirical calculations, DFT methods can provide unambiguous results on structural and dynamic properties of small- to medium-size molecules. These calculations are sufficiently accurate, include correlation and exchange effects, and at the same time are faster than other methods. In conjunction with the Car–Parrinello approach⁷ of combined electronic and nuclear coordinates optimization, this class of techniques is capable of calculating static and dynamic properties of large organic molecules in excellent agreement with experiments.^{4,8,9} Due to limitations in computer power, *ab initio*-only techniques cannot be applied in the time being to tackle problems involving long time and large length scales, but can provide an essential modeling tool for classical simulation methods such as molecular dynamics (MD), which are better suited for that task. Indeed, *ab initio* methods constitute the underpinning of the modern force fields for biologic molecules such as proteins, DNA, and RNA.

Much in the same spirit, this article presents a comprehensive classical force field for the cofactors of bacterial photosynthesis, based on high-quality *ab initio* DFT calculations. In our investigation an extensive set of structural and dynamical data was obtained from DFT as reference data to test and refine a molecular mechanics (MM) models of methyl bacteriochlorophyll (BChl) and bacteriopheophytin (BPh) *a*, and of a derivative of ubiquinone (U10). The structure and dynamics of the cofactors, their potential energy surface, and their behavior in the condensed phase predicted by the new force field are in good agreement with both DFT and experimental results. We stress that our new force field for photosynthetic cofactors is the first to appear in the open literature based on a reliable set of reference data and following closely the AMBER potential parameters development scheme.¹⁰ Thus, it can be used in combination with the AMBER force field to simulate the cofactors in a protein environment. Simulations of bacterial photosynthesis in the reaction center protein with our new force field have already been successfully carried out.¹¹

The article is organized as follows: In the next section we present the techniques and methods used in our *ab initio* calculation and classical molecular modeling. Then in succeeding sections we define and discuss all the potential parameters of the force field for bacteriochlorophylls, quinone, and of their phytyl chain, respectively. The same sections also provide details of the DFT calculations and of their results vis-à-vis the experimental structure and spectra. The article ends with a summary and conclusions.

Methods and Force Field Refinement

In this investigation, the general strategy for force field development has followed a scheme similar in spirit to that applied to amino acids and DNA bases to obtain AMBER.¹⁰ Thus, to describe bonded and nonbonded contributions our investigation used the AMBER potential function, defined as:

$$V(\vec{R}) = \sum_{stre.} k_b(b - b_0)^2 + \sum_{bend.} k_\theta(\theta - \theta_0)^2$$

$$+ \sum_{tors.} K_\phi(1 + \cos(n_\phi\phi + \delta_\phi)) + \sum_{impr.} k_\omega(1 + \cos(n_\omega\omega + \delta_\omega)) + \sum_{i,j} 4\epsilon_{i,j} \left[\left(\frac{\sigma_{ij}}{r_{ij}} \right)^{12} - \left(\frac{\sigma_{ij}}{r_{ij}} \right)^6 \right] + \sum_{i,j} \frac{q_i q_j}{r_{ij}} \quad (1)$$

In this functional form, a force constant and an equilibrium value define the force field for bond stretching (K_b, b_0) and bond angles (K_θ, θ_0), while the force constants, K_ϕ and K_ω , with the multiplicity factors, n_ϕ and n_ω , are necessary for proper torsions along with corresponding phase factors, δ_ϕ and δ_ω , which are either 0 or 180°. Finally, dispersions and electrostatics interactions are handled by Lennard–Jones functions and point charge Coulombic potentials, respectively.

The departure points of our force field development have been the existing AMBER potential parameters for the small fragments that form the bacteriochlorophylls and quinones found in the photosynthetic RC. Unfortunately, the RC cofactors are in part composed of some unique molecular fragments not included in the AMBER database for which an *ex novo ab initio*-based modelization was performed.

To complicate matter furtherly, the direct extension of the fragment parameters always need additional refinement when fragments are part of a topologically complex compound. Thus, DFT *ab initio* calculations were also carried out on the entire RC cofactors to optimize their structures and compute their vibrational normal modes. These data were used first to fit atomic partial charges and then to refine the bonded part of the potential parameters.

As a final step, experimental data from X-ray crystallography were used, when available, to check the structural properties in the condensed state and to further refine the intermolecular parameters. Because only the X-ray structure of a derivative of BPh—the Methylbacteriopheophorbide (MeBPh) with benzene¹²—is known, we used this structure as the reference of our potential refinement.

In the following sections we discuss in details the techniques and methods used to construct the force field for the RC cofactors.

DFT Calculations

In the past, *ab initio* calculations based on the Density Functional Theory (DFT) approximation have been gaining popularity for the application to biological and chemical systems.^{8,13} Indeed, these calculations are faster than other methods and, at the same time, accurate—including correlation and exchange effects. In conjunction with the Car–Parrinello approach⁷ of combined electronic and nuclear coordinates optimization, this class of techniques is capable of calculating nuclear positions of complex molecules in excellent agreement with experimental X-ray structures.^{4,9,14} In particular, *ab initio* DFT methods have been applied successfully to calculate structural properties of a bacteriochlorophyll derivative—the *a* type methyl bacteriopheophytins or MeBPh *a*.^{4,15}

In this work, we have extended the *ab initio* investigation to the determination and assignment of the normal modes of methyl bacteriochlorophyll *a*, for which a first account was published on ref. 6, and of an ubiquinone derivative. Those results were used in the molecular modeling of RC cofactors described in this article.

An additional part of this *ab initio* database are data obtained from DFT calculations of an isolated methyl acetate (MeA) molecule representative of two side chains attached to ring IV and V of chlorophylls.

In our investigation, the electron ground state energy as a function of the atomic coordinates $\{\mathbf{R}_i\}$ is computed within density functional theory¹⁶ with the gradient corrected approximation of Perdew and Becke^{17,18} for the exchange and correlation energy. This approximation has been chosen because it is known to provide a fairly accurate description of hydrogen bonds.¹⁹ In our computation only valence electrons are treated explicitly, and their interaction with the ionic cores is described by soft pseudopotentials of the Troullier–Martins type.²⁰ The Kohn–Sham orbitals are expanded on a basis of plane waves, with a kinetic energy cutoff of 70 Ry, while the first Brillouin zone is sampled at the Γ -point only. In view of the insulating character of this compound, and of the relatively large size of the unit cell (39 to 86 atoms), this approximation is expected to have negligible influence on the computed properties.²¹ In the case of the gas phase molecule, the volume of the periodically repeated unit cell ($V = 9500 \text{ \AA}^3$) is such that the interaction of the central molecule with the periodic replicas is negligible. For all molecules discussed here, the calculations were carried out in a cell of 18 \AA .

The atomic positions are relaxed by the DFT–molecular dynamics scheme of Car and Parrinello⁷ using a simulated annealing procedure. The relaxation is continued until the residual forces on the atoms drop below a preassigned threshold, that, in the present computation is set to 10^{-5} in atomic units.

The *ab initio* vibrational modes were computed by diagonalizing a finite difference approximation for the dynamical matrix using the first derivatives of the energy close to the minimum of the energy. The assignment was done using a set of internal coordinates and based on the M-matrix method.²² For the ubiquinone molecule, the energy profiles of a few dihedral angles were calculated by constraining the angles at selected values in the appropriate range during structure optimization.

All DFT *ab initio* calculations of this investigation were carried out with the CPMD program.²³

Force Field Refinement

The first step in developing a force field for RC cofactors was to derive their electrostatic potential field directly from *ab initio*. We then assigned to each atom a Lennard–Jones dispersion interaction taken straightforwardly from AMBER. With this initial set of parameters in place we refined the bonded forces terms of the potential against *ab initio* results on the structure and dynamics of the cofactors *in vacuo*. Then, dihedral force parameters of few unhindered lateral chains were derived by direct comparison of the *ab initio* and classical force field energy profiles. Finally, simulations in condensed phases were carried out to check and verify the potential parameters.

Electrostatic and Nonbonded Forces

Electrostatics was handled in our model with a set of partial charges assigned to each atom. These charges can be derived by at least two different schemes: fit to *ab initio* electrostatic potential

on a set of grid points around the molecule (ESP, or Electrostatic Potential-based techniques²⁴) or population analysis. In this investigation only charges derived by Mulliken population analysis were used. This approach provides a set of charges obtained by projecting the Kohn–Sham eigenstates onto a minimal basis of pseudoatomic wave functions. To correct for the unassigned charges, the Mulliken charges (MULL) of H, C, N, and O are rescaled by constant factors to achieve charge neutrality and to reproduce the three Cartesian components of the dipole moment given by the *ab initio* computation.

By construction, the ESP charges reproduce quite accurately, in a mean square sense, the higher electrostatic moments. This is not the case of the Mulliken charges, which in principle, can reproduce only the first moment, the dipole.

Bonds and Angles

The refinement of bond and angle force parameters in eq. (1) is crucial to reproduce the local structure and the fastest vibrations of the molecule. In our approach, a special stress was placed on reproducing both the molecular *ab initio* frequencies and eigenvectors. This was done with the intention to producing a simple classical force field close to spectroscopic quality.

To obtain this result, after a first optimization of parameters to fit bond and angles equilibrium values, frequencies, and eigenvectors were refined by iterative optimization of the force constants. This adjustment was performed by hand to avoid any combination of “unphysical” parameters that reproduce the reference data.²⁵ Because of the correlation between force constants and equilibrium values, these optimizations were performed self-consistently with several cycles involving adjustment of force constants followed by new refinement of equilibrium values until convergence of both structural and dynamical data was achieved.

Dihedrals

Dihedral angle terms in eq. (1) should reproduce the rotation of chemical groups around bonds and out-of-plane modes. When atoms chemically constrained on a ring are considered, rotations are hindered while only deformations are possible. When, instead, rotations around a bond was possible, *ab initio* calculations were carried out to derive the potential energy profile for that torsional rotation. This was carried out by optimizing the system structure with a constraint on the dihedral angle. MM force constants were then refined to reproduce that barrier and its symmetry. This is achieved with one or more cosine functions, changing the multiplicity parameter n_ϕ and the force constants K_ϕ [see eq. (1)]. In some case, more than one Fourier term was needed to reproduce the energy barrier.

Molecular Mechanics and Simulation

Structural minimization is essential in our refinement process. Indeed, each parameter modification must be followed by an energy minimization to obtain the structural parameters and the normal modes. Because of the complexity of the systems investigated here and the large number of nearly equivalent isomers generated by rotation of the numerous external groups, we used

preferentially simulated annealing (SA) techniques to obtain the global minimum. Several cycles of minimization were carried out: after a few picoseconds at 300 K in the NVE ensemble, we used the molecular dynamics (MD)-based SA scheme to arrive at low temperature, followed by a conjugate gradient (CG) method to minimize further. In the end the CG method arrived in all cases studied at a gradient less than 10^{-7} kcal/mol \AA^{-1} . Subsequent to minimizations, the dynamical matrix in Cartesian coordinates was computed by numerically evaluating the second derivative of the potential at the minimum of the total energy.²⁶ Then, the computed normal modes were transformed into a set of nonredundant internal coordinates,²⁷ and the assignment of the normal modes was carried out based on the M-matrix method.²² This technique provides a description of each frequency as a combination of internal modes that correspond to energy terms in eq. (1), i.e. stretchings, bendings, and torsions.

Condensed phase simulations in the isobaric-isothermal (NPT) ensemble were carried out with the extended system approach that involves adding extra dynamical variables to the systems to control temperature and pressure.^{28–31} Although other approaches are possible,³² only techniques of this class are able to generate the desired equilibrium distribution functions. Throughout this study NPT simulations were carried out using the atom group scaling algorithm fully described in ref. 33 and implemented in our MD program ORAC.³⁴ The integration of the equations of motions is achieved using a five time steps scheme with a Liouvillean separation in three nonbonded shells, with particle mesh Ewald^{35,36} to handle electrostatic interactions, and constraints on covalent bonds entailing hydrogens.³⁷ The computational advantage of using constraints on covalent hydrogen bonds is discussed in refs. 33 and 38.

Parametrization of Bacteriochlorophylls

The most characteristic feature of bacteriochlorophylls and bacteriopheophytins (the dihydro metal-free derivative of BChl) is their tetrapyrrolic architecture related directly to metalloporphyrin. These molecules differ remarkably from the latter because of the broken symmetry created by the presence of the ring V and the saturation of ring II and IV (see Fig. 1). Around their imidazole ring structure are numerous lateral chains: Two methyl acetate groups (MeA) attached to rings IV and V; several methylic groups; one carboxyl group attached to ring I; and a phytol chain composed of four isoprene units attached to ring IV.

Ab initio calculations *in vacuo* were carried out for both BChl and BPh. To decrease the number of degrees of freedom, a large part of the phytol chain was cut. The effect of this simplification on the structural properties seems to be small as demonstrated in recent calculations of chemical shifts on BChl and BPh.¹⁵ Thus, the final systems investigated by *ab initio* calculation were composed of 85 and 86 atoms for BChl and BPh, respectively. Calculations were also carried out on MeA and pyrrole, these being the principal components of BChl and BPh. Data for pyrrole ring were also taken from literature.³⁹

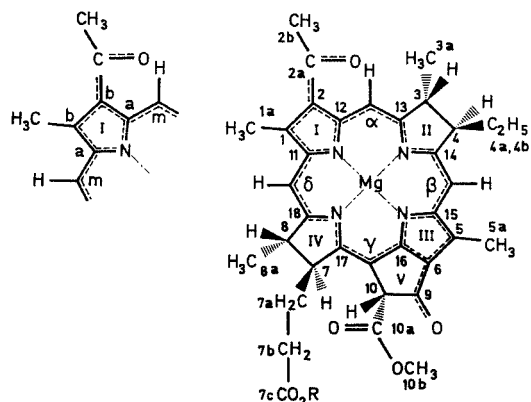


Figure 1. Chemical structure of methyl bacteriochlorophyll *a*, with $R = \text{CH}_3$. On the right: numbering of carbon atoms according to the Fischer system. On the left: generic labeling of meso and pyrrolic carbon atoms.

DFT Results

Static Properties

In general, the optimized coordinates obtained from *ab initio* DFT techniques such as those used in this article are always in good agreement with X-ray determined structures. Specifically, for the small MeA molecule we found deviations less than 0.01 \AA for bond lengths and less than 1° for bond angles found in literature.^{40,41} For BPh structural results can be compared with the X-ray structure of MeBph.¹² Taking as reference data the X-ray distances and angles of MeBph, average deviations of 0.025 \AA for bond lengths and 1° for bond angles involving only carbons and nitrogens were obtained for BPh. Given the complexity of this class of molecules and the large number of minima due to possible isomerization of the lateral groups the deviation from experimental structures is larger than for smaller molecules. In particular, the global root-mean-square deviation (RMS) on heavy (nonhydrogen) atoms of BPh is found close to 0.1–0.2 \AA . The quantity RMS is defined as

$$\text{RMS} = \min \left(\sum_i (r_i - r_i^{\text{X-ray}})^2 \right)^{1/2}, \quad (2)$$

where min implies the minimization of the sum—obtained by rigid body rotations and translation of one of the molecules. As shown in Table 1 an RMS of 0.048 \AA is obtained for the 26 atoms of the five rings and connections, the central body, and an RMS = 0.106 \AA for the other 20 heavy atoms for a total average of 0.089 \AA .

Another structural property investigated was the orientation of the central body relative to a plane (Z-plane) defined by the four nitrogens. The distance between the 26 atoms of the five rings and the molecular plane computed by DFT reveals deviations from planarity in good agreement with X-ray (see Fig. 2).

No relevant structural differences were found between current calculations on BPh and those reported in ref. 4, carried out on the MeBph crystal with different pseudopotentials and basis sets. Not

Table 1. RMS Deviations in Å for Structures *In Vacuo* of BPh and BChl Obtained from DFT or MM Optimization (Opt.).

System	Ref.	Opt.	All	Central	Side Chains
BChl	DFT	MM	0.213	0.060	0.439
BPh	X-ray	DFT	0.089	0.048	0.106
BPh	DFT	MM	0.241	0.089	0.461

The molecular rigid body fit (see explanations to Eq. 3 in the text) is on all the heavy atoms of the reference system (Ref.), i.e. X-ray or DFT structures. all: RMS deviations for all heavy (non-hydrogen) atoms. central: RMS deviations for the heavy atoms in the central body, namely the atoms of the imidazole ring, of the molecule. Lateral Chains: RMS deviation for the heavy atoms in external groups.

surprisingly, the optimized structures of BPh and BChl differ only in the region near the four nitrogens. The Mg in BChl distorts the pyrrole rings producing deviations from BChl of only a few degrees for the internal bending angles of rings. Deviations of less 0.1 Å, on average, were found for bonds.

Frequencies and Eigenvectors

The calculations of the normal modes by DFT provide information, essential for molecular modeling and not obtainable from experiment, such as eigenvalues and eigenvectors. DFT vibrational analysis was carried out only for the BChl molecule, the most studied experimentally, and not on BPh. Indeed, given the large mass of Mg, most of the normal modes of the BPh will not significantly differ from those of BChl, as vibrations involving Mg are well separated from other internal modes.

The DFT *ab initio* assignment of the resonant Raman spectra of BChl was presented in an earlier publication.⁶ In Tables 2 and 3 for all modes except C—H₃ stretchings and bendings we associate

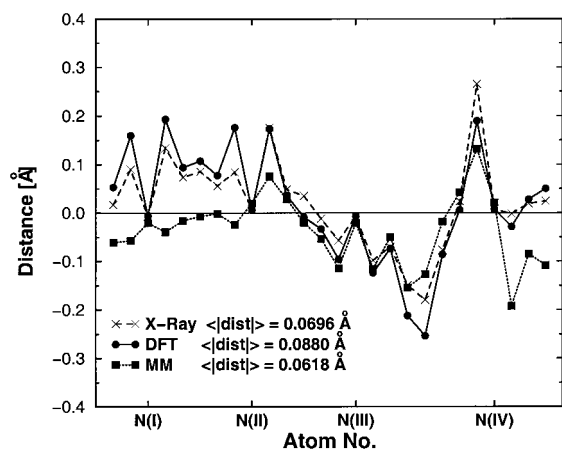


Figure 2. Distance between the 26 atoms of the five rings of BPh and the molecular plane for the DFT, MM and X-ray structures. In the left corner we show the average distance from the plane in Å for the three structures.

Table 2. Comparison of the DFT Stretchings Frequencies with Those Obtained from the MM Model.

Mode	Ring No.	DFT	MM
as νC_a-C_a		1571, 1613, 1633	1611, 1619
as νC_a-C_β		1571, 1613, 1633	1594, 1619, 1624
as νC_a-C_γ		1580, 1613, 1633	1594, 1611, 1624
as νC_a-C_δ		1580, 1613, 1633	1619, 1624
s νC_a-C_a		1463	—
s νC_a-C_β		1446	—
s νC_a-C_γ		1512, 1544	225, 1546
s νC_a-C_δ		1457	—
$\nu C-N$	I	1127, 1383	—
	I	1390	—
	II	1463	—
	II	1446	—
	III	1138, 1349	—
	III	1512, 1544	1546
	IV	1298	—
	IV	1457	—
νC_a-C_b	I	—	—
	I	—	—
	II	—	—
	II	965	—
	III	—	—
	III	1422, 1444	—
	IV	889, 1298	—
	IV	868	782
	V	—	—
νC_b-C_b	I	1498	—
	II	921, 1099	1017
	III	1512, 1544	1514, 1546
	IV	889, 1099	—
	V	—	—
	V	601	585
Ext. $\nu C-C$	I	—	540
	I	409	414
	I	944	—
	III	1139	545
	IV	839, 1159	558
	V	976	853
$\nu C=O$			
Keto		1718, 1732	1719
	I	1648	1664
	IV	1737	1738, 1739
	V	1718, 1732	1738, 1739
$\nu C-O$	IV	593, 983	737
	IV	905, 983	1009
	V	906, 1118	—
	V	906, 952, 976	1007, 1470
$\nu Mg-N$		443, 491	419

In the table, ν -labels stretching, “s” stands for symmetric, and “as” for antisymmetric. In case modes assigned to stretching of bond between identical atom types, but occurring on different rings, the Roman number of the ring is used to classify the mode. Atom labels in the table are defined in Figure 1.

Table 3. Comparison of the DFT Bending and Out of Plane Frequencies with Those Obtained from the MM Model.

Mode	Ring No.	DFT	MM
s $\delta\text{N}-\text{C}-\text{C}_\alpha$		733	636
as $\delta\text{N}-\text{C}-\text{C}_\alpha$		261	—
s $\delta\text{N}-\text{C}-\text{C}_\beta$		898	—
as $\delta\text{N}-\text{C}-\text{C}_\beta$		—	—
s $\delta\text{N}-\text{C}-\text{C}_\gamma$		—	—
as $\delta\text{N}-\text{C}-\text{C}_\gamma$		550	—
s $\delta\text{N}-\text{C}-\text{C}_\delta$		912	—
as $\delta\text{N}-\text{C}-\text{C}_\delta$		—	—
δ	I	704	656
	I	603	—
	II	—	801
	II	601	504
	III	774, 780, 1113	—
	III	550	427
	IV	780	782
	IV	686	603
	V	—	—
$\delta\text{C}-\text{C}_\alpha\text{H}$		1182, 1390	1299, 1315, 1355
$\delta\text{C}-\text{C}_\beta\text{H}$		1349	1080, 1207
$\delta\text{C}-\text{C}_\delta\text{H}$		1190, 1370, 1383	1235
$\delta\text{C}-\text{C}-\text{C}$			
Ext.	I	307, 579	—
	I	250, 261	403
	III	137	325, 375
$\delta\text{C}=\text{O}$ Keto		491, 828	—
	I	579, 603	—
	I	261, 359	—
	IV	593, 839	558
	IV	—	327, 445, 450
	V	—	670, 693
	V	284, 906	273
$\delta\text{C}-\text{O}-\text{C}$	IV	345, 367, 839	322, 327, 333
	V	326, 351	365, 371
$\delta\text{C}-\text{N}-\text{Mg}$		321, 387	480, 545
$\gamma\text{C}-\text{C}_\alpha$		756	—
$\gamma\text{C}-\text{C}_\alpha$		695	119
$\gamma\text{C}-\text{C}_\beta$		635	116
$\gamma\text{C}-\text{C}_\beta$		730	670
$\gamma\text{C}-\text{C}_\gamma$		752, 780	—
$\gamma\text{C}-\text{C}_\gamma$		113, 669	—
$\gamma\text{C}-\text{C}_\delta$		93, 669	119
$\gamma\text{C}-\text{C}_\delta$		739	660
			812, 929, 947,
$\gamma\text{C}_\alpha-\text{H}$		930	1018
$\gamma\text{C}_\beta-\text{H}$		853, 865	971, 994
$\gamma\text{C}_\delta-\text{H}$		854	961, 973
$\gamma\text{C}_\gamma-\text{C}$		780	232, 853
$\gamma\text{C}=\text{O}$ Keto		643, 828	518, 614
	I	603, 622, 1007	1018
	IV	593, 660	737, 819
	V	643, 752, 828	808
γMg		190, 195	309

See Table 2 for explanations of the symbols.

their predominant internal coordinates. Contributions from coordinates weighting less than 10% in the eigenvectors were ignored. Two different classes of modes can be distinguished: In plane (IP) modes at higher frequencies and out of plane (OOP) mode at lower frequencies, below 1020 cm^{-1} .

If C—H stretching are excluded, we find that the highest IP frequencies of BChl are C=O stretchings in the range $1740\text{--}1650\text{ cm}^{-1}$. Lower in the $1634\text{--}1447\text{ cm}^{-1}$ region, near the $\text{C}_{2a}=\text{O}$ acetyl stretching at 1648 cm^{-1} , another IP fundamental region is found that includes predominantly C_aC_m , C_bC_b , and CN stretchings (see Fig. 1). Symmetries of these modes are discussed in ref. 6. Below 1447 cm^{-1} down to 1114 , many modes are found involving a contribution from νCN , but mixed strongly with the predominant C—H₃ bendings.

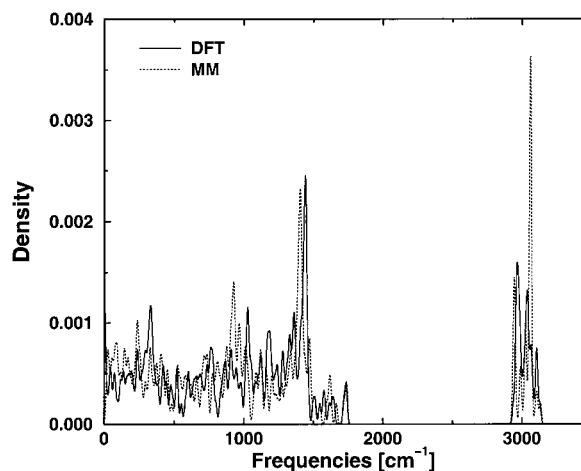
No significant symmetries were found instead for OOP modes. As shown in Figure 4, the highest frequencies, in the range of $500\text{--}1000\text{ cm}^{-1}$, involve modes localized at the base of the two unsaturated pyrrol rings and coupled with external groups. In the range $200\text{--}400\text{ cm}^{-1}$, modes involving Mg, N, and C of the central molecular body are found instead.

Although the main focus here is on BChl, DFT computation of normal modes was also performed on MeA and pyrrole. For the two molecules we find vibrational frequencies in good agreement with experimental values^{40,41} with average deviations of about 2.3%. In MeA, poorer agreement was found only for two particular frequencies identified as rocking in C—H₃ groups at 1000 cm^{-1} , where the deviations is 8.5%.

Parametrization

Intramolecular Parametrization

In building the force field for BChl and BPh we have limited the new types of atoms added to AMBER to the bare minimum. Nonetheless, to parametrize the new force field a total of 22 types were needed, as shown in Figure 5. Given the similarity between the two molecular structures the same atom type is used for

**Figure 3.** Comparison of the DFT and MM spectral density of BChl obtained from normal mode analysis.

densities of states computed with MM and DFT is presented in Figure 3.

Good agreement between MM and DFT is found for all the regions of the spectrum, although discrepancies are larger in the region near 1000 cm^{-1} . In the MM model the group of frequencies involving the hydrogen bendings falls at around 920 cm^{-1} , which compares with a DFT peak at higher frequency, 1020 cm^{-1} . We found that a better match could be achieved with larger force constants for bendings involving hydrogens. Unfortunately, these modifications would also shift unfavorably the hydrogen bending peak at higher frequency near 1400 cm^{-1} , by mixing these modes with vibrations involving atoms of the macrocycle in the region above 1450 cm^{-1} . Given the importance of the coupling between these frequencies with electronic properties,⁶ these force field modifications were not retained in the final parameter set.

Not surprisingly, the fit of the DFT computed BChl eigenvectors is much harder than the fit of the eigenvalues. Indeed, attempt to devised automated procedures for eigenvectors fitting might give unphysical results,²⁵ especially for complex molecules. Our approach here used the following procedure: After a first refinement of the force constants to give a good match for the several region of the DFT spectrum, we selected a set of eigenvectors that we defined “characteristic” for our molecules. We chose all the eigenvectors of the $1450\text{--}1700\text{ cm}^{-1}$ region, a few CN and CO stretchings and some OOP modes involving the CO groups, the CH methine bridge groups and the CCH_3 groups at the base of the pyrrolic rings (I and III). We then refined the force constants to reproduce the corresponding DFT eigenvectors.

In Figure 4 we compare the final molecular modeling results for the region $1450\text{--}1650\text{ cm}^{-1}$ and for some OOP modes in the region $200\text{--}1000\text{ cm}^{-1}$. In the first set of vibrations, Figure 4a, four modes are delocalized on the eight $\text{C}_a\text{--C}_m$ bonds of the macrocycle. To obtain this behavior the choice of force field parameters is somewhat counterintuitive. Indeed, identical stretching force constants for all the $\text{C}_a\text{--C}_m$ bonds only give rise to modes localized on the four $\text{C}_a\text{--C}_m\text{--C}_a$ groups, with the highest frequency localized between rings III–IV (methine carbon C_γ). To obtain the DFT delocalization, larger force constants were needed for shorter $\text{C}_a\text{--C}_m$ bond lengths. Thus, force constants of 370, 350, and $315\text{ kcal}/\text{\AA}^2$ were used for the $\text{C}_a\text{--C}_m$ bonds attached to the saturated rings, to pyrrole rings and for bonds of the Vth ring, respectively. This choice of force constants is consistent with $\text{C}_a\text{--C}_m$ DFT bonds, that are shorter, and hence stronger, if attached to saturated rings (ring II and IV) than to unsaturated pyrrole rings (ring I and III).

It is interesting to notice that smaller stretching constants are compensated by an increased coupling of $\text{C}_a\text{--C}_m$ with $\text{C}_a\text{--C}_b$. Indeed, $\text{C}_a\text{--C}_b$ bonds have distances near 1.45 \AA for ring I and III, which contrasts with 1.52 \AA for ring II and IV. Also, the force constant relative to the bend $\text{C}_a\text{--N--C}_a$ is large, i.e., $120\text{ kcal}/\text{deg}^2$, compared with bending parameters used in AMBER to describe pyrrol rings. This also contributes to the delocalization of the modes by bridging the $\text{C}_a\text{--C}_m$ bonds of the macrocycle.

The remaining modes in the region $1450\text{--}1550\text{ cm}^{-1}$ are localized on the $\text{C}_b\text{--C}_b$ and $\text{C}_a\text{--N}$ of the unsaturated pyrrole rings, I and IV, and in the region of the ring V and the acetyl group, (see Fig. 4b). In Figure 4c, OOP modes involving the Mg atoms

are also shown. The good agreement between DFT and MM eigenvectors was achieved without new special parameters.

In Tables 2–3 we compared the assignment of DFT and MM frequencies found for each type of internal mode of BChl. We assigned a frequency to a stretching or bending mode only when such a mode is dominant, i.e., its participation ratio is larger than 10%. Although this comparison is more quantitative than a direct inspection of the eigenvectors from Figure 4, several MM internal modes do not belong, in this context, to any specific class of DFT modes—this limits somewhat the use of the M-matrix method. Consequently, Tables 2–3 illustrate that for each type of internal modes the range of the assigned frequencies obtained with our MM model is sufficiently close to the DFT result.

It is important to point out here that a one-to-one comparison of frequencies is very difficult for large molecules where, as it is the case in BChl, the degree of mode mixing is high. Thus, only in a few instances—for some specific molecular groups—a direct comparison between DFT and MM frequencies is possible. A first ensemble of modes involves the methyl-acetate groups, the keto oxygen, and the acetyl group. As these groups are spatially isolated from the central imidazole ring of the molecule, the MM–DFT comparison of the frequencies is simpler, and an RMS deviation of 9, 26, and 35 cm^{-1} is obtained for the stretchings, bendings, and out-of-plane modes of the C=O groups, respectively. On the other hand, the C--O frequencies are more influenced by the environment yielding larger RMS deviations, with 105 and 29 cm^{-1} obtained for stretchings and bendings—the stretching modes mix with CH_3 bendings found at similar energies. The methine bridge groups have RMS deviations of 15, 77, and 95 cm^{-1} for stretchings, bendings, and out-of-plane modes, respectively. This somewhat larger deviation might be due to the topologically complex embedding environment. For the pyrrole rings (I and III) the RMS deviation for stretchings involving the base of the ring is smaller, at about 47 cm^{-1} . Also, in the group of frequencies involving Mg we have 24, 150, and 110 cm^{-1} RMS deviations for stretchings, bendings, and out of plane, respectively. Finally, the direct comparison of the CN group of frequencies was not possible, as their large mixing with the CH_3 bendings does not allow a good resolution with the M-matrix method.

Intermolecular Interactions

After the force field parameters were refined against single molecule structural and dynamic properties, the resulting set was tested to reproduce structural properties in the condensed phase. Constant pressure and temperature molecular dynamics (MD) techniques were used to simulate the crystal derivative of BChl, MeBph, the structure of which is known.¹² MeBph crystallizes at 200 K with a solvation benzene molecule in the triclinic space group P1, with $a = 7.184\text{ \AA}$, $b = 8.073\text{ \AA}$, $c = 17.071\text{ \AA}$, $\alpha = 91.04^\circ$, $\beta = 93.50^\circ$, $\gamma = 110.06^\circ$, $V = 927.43\text{ \AA}^3$. To simulate the MeBph crystal, our MD simulation box contained a supercell obtained by replicating the crystal unit cell $4 \times 4 \times 2$ times, in the three directions, for a total of 3136 atoms and cell constants $a = 28.736$, $b = 32.292$, and $c = 34.142\text{ \AA}$, with the total volume, $V = 29678\text{ \AA}^3$.

This system was initially relaxed in the NVE ensemble at low temperature, $T = 20\text{ K}$, for 3 ps and then slowly heated to 200 K.

Table 4. Volumes and Cell Parameters for the 32 Unit Cell of MeBph in Benzene.

System	$\langle \text{Volume} \rangle$	$\langle X \rangle$	$\langle Y \rangle$	$\langle Z \rangle$	$\langle \alpha \rangle$	$\langle \beta \rangle$	$\langle \gamma \rangle$
EXP.	29678 Å ³	28.7 Å	32.3 Å	34.1 Å	91.0°	93.5°	110.1°
ESP	31164	28.8	33.4	35.1	90.7	94.9	111.7
MULL	30959	29.3	33.3	34.2	91.9	94.6	111.1
ESP + LJ	29802	28.1	32.8	34.7	90.5	94.2	111.2

Experimental X-ray values are compared with averages over 50 ps of an MD simulations at 200 K.

Bonds involving hydrogen atoms were kept rigid by constraint techniques.^{42,43} Finally, three simulations in the NPT ensemble were performed at 200 K and with $P = 0.1$ MPa, which lasted 100 ps each, including an initial equilibration period of 50 ps. Configurations were collected for analysis every 25 fs. Additional 30 ps runs were also carried out without the bond constraints to compute the vibrational density of states of the molecules.

The three independent 100 ps trajectories used three different nonbonded parameters: (1) ESP trajectory carried out with ESP charges; (2) MULL trajectory involving Mulliken charges; (3) ESP-LJ trajectory carried out with ESP charges and modified Lennard-Jones parameters where σ s on all hydrogens bound to methyl carbons were reduced by 9%.

Two different types of structural RMS differences were performed: (1) a RMS deviation between the initial MD box, generated by replicating the X-ray cell, and the simulated instantaneous MD box, or *cell fit*; (2) a RMS deviation of each simulated MeBph molecule from its X-ray coordinates, or *single molecule fit*. These calculations were all preceded by rigid body fits of the two structures considered, such fits including only contributions from heavy atoms. The RMS computed through a *single molecule fit* was averaged over the 32 MeBph molecules of the simulation box. The comparison of results obtained with the two types of rigid body fit allows to discriminate the behavior of the nonbonded parameter sets against reproduction of intermolecular and intramolecular structural features.

Condensed Phase Simulations

We first notice that for all the nonbonded parameters sets (ESP, MULL, and ESP-LJ) used here the cell parameters deviated little

Table 5. RMS Deviations in Å between the X-ray Ideal Cell and the MD Simulation Box.

System	All	MeBph	Benzene
ESP	0.889	0.470	1.535
MULL	0.829	0.379	1.455
ESP + LJ	0.851	0.363	1.523

The RMSs are obtained by taking the mean instantaneous deviation between the simulated 32 MeBph unitary cells and the X-ray. The RMSs are then averaged over the 50 ps run. “all” implies averages over the heavy atoms of MeBph and benzene, while “MeBph” and “Benzene” include contribution from heavy atoms of only the MeBph and benzene, respectively. ESP, MULL, ESP-LJ refer to trajectories carried out with different electrostatic and nonbonded potentials as described in the text.

along the whole temporal trajectory, while for trajectories ESP and MULL relative differences with experimental cell volume are at most 5% (see Table 4).

Data in Table 5, which reports the *cell fit* RMS deviations, show that benzene is much more mobile than the MeBph molecules with a few of the 32 benzenes behaving like free rotors at 200 K. From the same table, differences in the RMS of MeBph for the three trajectories are correlated with the volume cell differences. Indeed, the ESP trajectories, predicting the largest cell volumes, show bigger RMS deviations than the ESP-LJ trajectory for which special parameters were devised to fit the experimental volume. Although the ESP-LJ trajectory produce the best agreement with the crystal volume, we remark that the corresponding RMS deviations from the *single molecule fit* increased for all atoms compared to the ESP result. Different behavior is found for the MULL trajectory where a larger volume is found with respect to ESP-LJ, while less mobile benzenes are the cause of a small *cell fit* RMS.

The RMS deviations obtained in Table 6 with *single molecule fit* show that the crystal environment prevented large displacements of external groups relative to calculations in vacuum. The ESP trajectory shows the best agreement with the X-ray structure of MeBph, while the RMS’s of MULL and ESP-LJ are slightly higher. Figure 6 presents the RMS deviation of each molecule in the unit cell. Here, MULL RMS deviations are smaller than ESP and ESP-LJ for all molecules except two for which large deviations are seen. This behavior is caused by lateral chains rotations occurring during the simulation, which are very rare for the MULL trajectory (only two molecules experience such a transition), but

Table 6. RMS Deviations in Å between the X-ray Structure and the MM Model.

System	Simulation	All	Central	Lateral Chains
ESP	min.	0.247	0.089	0.472
MULL	min.	0.277	0.113	0.509
ESP + LJ	min.	0.259	0.100	0.486
ESP	NPT	0.238	0.150	0.360
MULL	NPT	0.210	0.141	0.310
ESP + LJ	NPT	0.250	0.148	0.395

Results were obtained from *in vacuo* minimizations (min.) and condensed phase MD NPT simulation (NPT). all, “Central” and “Lateral Chains” have all the same meaning as in Table I. Also ESP, MULL, ESP-LJ refer to trajectories obtained with different potentials as explained in the text.

cq0 and cq2. Only one additional type was needed to model the phytyl chain (cq); see Fig. 7). To reproduce DFT frequencies, eigenvectors and torsional profiles discussed down below, 11 stretchings, 25 bendings, and 27 torsions were added to our MM force field.

Our parametrization followed the procedure used to model BChl and BPh. As for chlorophylls, our MM model of U10 involved ESP charges determined from additional *ab initio* calculations on a DFT optimized structure of U10, and the unmodified Lennard–Jones parameters of the AMBER force field. Then, structural data obtained from DFT optimization were used initially to derive the equilibrium distances and angle bendings of our potential. After a few parameter adjustments, the RMS deviation between the optimized MM and DFT structures reached 0.152 Å for the heavy atoms. As for BChl and BPh, the force constants were then refined to reproduce DFT frequencies and eigenvectors. In Table 9 we have classified each of the normal modes with its

Table 7. Assignment of the U10 DFT Frequencies from 1666 to 616 cm^{-1} with Comparison with IR Data.

Experimental	DFT	M-Matrix Assignment
1664	1666	C=O (86)
	1658	C=C _P (72)
1614	1643	C=C (42) C=O (24)
1644	1635	C=O (66) C=C (17)
	1585	C=C (57) C—O sym (15) C=O (12)
1288	1284	C—C asym (59) C—O sym (13)
1266	1244	C—O asym (17)
1208	1175	C—CT _P (33)
1156	1142	C—CT _R (18) C—O asym (17)
	1096	C—CT _P (13)
1096	1093	C—O asym (18)
1034	1028	C—CT _P (25)
	1017	C—CT _P (20)
	1003	C—CT _E (12) O—CT (11)
	984	CT—CT _P (22)
	932	CT—CT _P (19) O—CT (10) C—CT _P (10)
	926	O—CT (22)
	918	δ C—O (10)
	908	O—CT (51)
	862	γ C—H _P (37)
	830	γ C—H _P (12)
	811	γ C=O (31)
	793	γ C=O (16)
	786	C—CT _P (20)
	750	γ C=O (76)
	705	δ C=O (23) C—C sym (10)
	682	γ C—O (34) δ Ring (12)
	616	δ Ring (27)

δ labels bendings, if only two atoms are indicated the first one is the central atom. γ labels out-of-plane modes with the last atom moving out-of-plane. Finally τ labels torsions, only the atoms of the central bonds are indicated. The subscript *P* stands for modes of the phytyl chain. The subscript *E* refers instead to frequencies of the methyl group attached to the ring. The subscript *R* refers to frequencies of the ring region connected to the phytyl.

Table 8. Assignment of the U10 DFT Frequencies from 578 to 26 cm^{-1} .

Experimental	DFT	M-Matrix Assignment
	578	γ C—H _P (13) δ Ring (11)
	554	γ C—H _P (20) γ C—CT _R (10)
	548	C—C sym (10)
	490	δ C—O—CT (14)
	475	δ Ring (34) δ C=O (10)
	453	δ C=O (15) δ C—O—CT (12) C—C asym (12)
	426	γ C—CT _E (23) δ C—C _P (14)
	418	δ Ring (12) δ C=O (17) δ C—C _P (16)
	391	δ C—C _P (23) γ C—O (10)
	371	δ C—CT _R (26) δ C—O—CT (12)
	367	δ Ring (18) δ C—O (24)
	345	δ C—O (12)
	334	δ C—CT _E (20) δ C—CT _R (12) δ C—O (10) τ C—CT _R (13)
	306	τ CT—CT _P (42) τ O—CT (14)
	302	δ C—CT _E (24) δ C—CT _R (12) δ C—CT—CT _P (16)
	291	τ O—CT (24) τ CT—CT _P (49)
	282	τ O—CT (28)
	260	τ Ring (44) τ C—O (12) δ C—O—CT (10)
	245	τ O—CT (81)
	233	τ Ring (45) τ C—O (29)
	231	δ C—O (24) τ C—CT _R (15)
	221	τ C—CT _P (53)
	199	τ C—CT _E (77) τ C—CT _P (12)
	182	τ C—CT _R (15) τ C—CT _P (36)
	175	τ Ring (13)
	160	τ Ring (18) δ C—H _P (16)
	145	τ Ring (35) τ C—O (32) δ C—O (10)
	127	τ Ring (23) τ C—O (19) δ CT—C _P (17)
	104	τ C—CT _R (10) τ C—CT _P (47)
	64	τ C—CT _P (32) τ C—C _P (60)
	26	τ Ring (31) τ C—CT _R (14) τ C—CT _P (13)

See previous table for explanation of the symbols.

dominant internal coordinate and compared results from DFT and our final MM force field. We notice that all groups of frequencies found with the MM model match remarkably the DFT data. This improved agreement with DFT is probably due to the smaller dimension of the U10 and its simpler topology. In particular, bond stretchings are reproduced with RMS deviations of 44, 86, and 76 cm^{-1} for double bond C=O and C=C, C—O and C—C and C—CT and O—CT, respectively. On the overall RMS deviations of between 25 and 105 cm^{-1} are found for angle bendings. Better agreement with DFT is found for torsions, with an RMS between 15 and 42 cm^{-1} . This improvement is probably a result of additional force field adjustments of the MM force field to reproduce the DFT torsional barriers of the isoprene and the metoxy groups.

Torsional Barrier: Isoprene Groups

The relative position of the phytyl chain with respect to the ring is controlled by the dihedral angle defined by the four atoms cq2–cq2–ct2–cq1 (see Fig. 7). A dihedral of the same class is also

Table 9. DFT Characteristic Frequencies of U10 Compared to the MM Model.

Stretchings		Bendings		Torsions		Out-of-Plane	
DFT	MM	DFT	MM	DFT	MM	DFT	MM
(C=O, C=C)		Ring-int		τ Ring		γ C=O	
1666	1695	682	539	260		811	837
1658	1664	616	485	233	203	793	727
1643	1621	578	419	175	189	750	504
1635	1565	475	398	160	170		γ C—O
1585	1525	418	340	145	131		837
		367	331	127	125	682	667
		260	292	26	37	391	389
(C—O, C—C)		δ (C—O, C=O)		τ (O—C, O—CT)		γ C—CT	
1584	1565	918	1063	306	340		667
1284	1472	705	712	291	331	554	501
1244	1285	475	439	282	260		
1142	1237	453	398	260	203		
1093	1120	418	375	245	189		
705	780	367	344	233	170		
548		345	300	145	125		
453	485	334	268	127	85		
		231	260				γ C—C
		145	236	334		578	568
(O—CT, C—CT)		δ (C—CT, O—CT)		τ C—CT			
1175	1139	490	568	306		554	539
1142	1063	453	501	291	260		468
1096	1017	371	389	221	203	182	186
1028	997	334	375	199	189		
1017	983	302	344	182	170		
1003	972	260	268	104	70		
984	899			64	48		
932	854	δ C—C		τ C—C		γ C—H	
926	844		568	64	48	862	854
908	780	426	468			830	837
786	693	429	429			578	
		391	389			554	

found in the isoprene groups of the phytyl chain—dihedral cq_2 – cq_2 – ct_2 – ct_2 . Given the importance of these torsions for the conformational stability of the phytyl chain, the DFT energy profile for the cq_2 – cq_2 – ct_2 – cq_2 dihedral angle was computed. Thus, a series of structural DFT optimizations were carried out for U10 by constraining the dihedral angle to a range of values from 0 to 360° with increment of 15°. The same calculations were also performed with the MM force field using, in the beginning, torsional parameters obtained for 2-methylpropene.⁴⁹ This parametrization giving very poor agreement with DFT, we set to zero the dihedral force constants of cq_2 – cq_2 – ct_2 – cq_2 and modeled the torsional energy profile by the electrostatic charge–charge interactions only. This provides a good agreement with DFT data, as shown in Figure 8, although the DFT asymmetry between the two minima at 90° and 270° is not reproduced by MM.

Torsional Barrier: Methoxy Groups

The barriers to torsional rotations around the C—O bond of the methoxy groups were investigated in by performing *ab initio* optimizations for a series of U10 conformations where the two

cq_0 – cq_2 – o_1c – ct_3 dihedrals, $\theta(1)$ and $\theta(2)$ indicated in Figure 7 were constrained to fixed values. Two series of constrained optimizations were carried out: first $\theta(1)$ was fixed to 180° while $\theta(2)$ was constrained at values in the range [0–120]° spaced of 30° from each other (Fig. 9a); Second, $\theta(1)$ and $\theta(2)$ were set at the same values in the range [0–120]° equispaced of 30° as before (see Fig. 9b). The MM force field was then fitted to reproduce these energy profiles. Five extra torsional force constants each with different periodicity [the parameter n in eq. (1) set to 1, 2, 3, 4, 6] were necessary to obtain a good agreement with DFT data, as shown in Figure 9a and b.

Parametrization of the Phytyl Chain

In this investigation, DFT calculations on BChl, BPh, and U10 has been carried out for model systems with truncated phytyl chains. Consequently, the modeling of the full chains requires some extra effort. For all RC cofactors, parameters for stretchings and bendings of the phytyl chain were taken directly from the parametrization

zation of U10 described earlier, for which DFT calculations were carried out including the first isoprene unit. The dihedral force constants (cqq-ct2, cqq-cq2, cq2-ct2, and cq2-ct3) were instead modeled by the parameter sets developed in the past for 2-methylpropene and *cis*-2-butene.⁴⁹ Indeed, these two molecules have the same chemical groups present in the isoprene group.

Charges for the first isoprene unit of U10 were taken directly from the DFT calculation. Given the large dimensions of the BChl and BPh molecules, no DFT calculation on a chlorophylls attached to an isoprene unit was carried out. Instead, ESP charges were determined from a DFT optimized structure of an isoprene unit attached to a methyl acetate group and saturated by a methyl group.

To complete the modeling, charges far away from the cofactor ring had to be determined. Indeed, the isoprene charges calculated in the truncated U10 system are strongly influenced by the quinone ring. Thus, DFT ESP charges computed for an isolated isoprene units (saturated with two hydrogens for a total of 18 atoms) were used to model the remaining phytyl chain charges for chlorophylls and the quinone.

Conclusion

In this article we have derived and tested an *ab initio* force field for the cofactors of bacterial photosynthesis. In addition to direct information about the molecular properties, we have used the extended set of structural and energy data provided by our DFT computations and by experiment to derive MM potential parameters for quinones and chlorophylls. Results presented in this article have shown that our force field is able to reproduce very well *ab initio* structural and dynamics properties of BChl, BPh, and U10. In particular, a complete normal mode assignment for BChl and U10 reveals the high degree of accord between DFT and MM eigenvectors. This good agreement between DFT and the MM models has been obtained without increasing to unmanageable numbers the atomic types that characterize the force field, thus limiting its complexity.

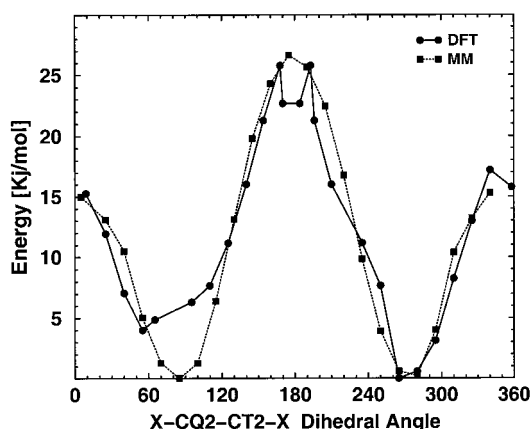


Figure 8. Energy profile for the C—CT barrier of U10. See text for explanation.

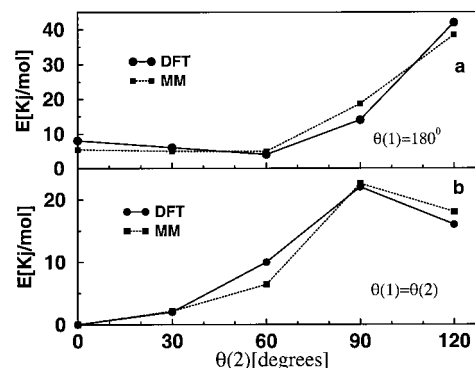


Figure 9. Energy profile for the C—O barriers of U10. See text for explanation.

The new force field has been developed following a scheme similar in spirit to that used by AMBER and is, thus, designed to be used in molecular dynamics simulations of photosynthetic proteins in association with the AMBER force field. Although in this investigation the use of the new force field in MD simulations has been restricted to a crystal of MeBph, successful simulations of the RC of *Rb. Sphaeroides* in a micellar environment has been already carried out—their results will be published in upcoming articles.¹¹ Given the stress placed in the refinement of the vibrational modes and eigenvectors, we think our parameter set also be useful to understand vibrational shifts due to changes in the protein environment as revealed by vibrational spectroscopies (FTIR and RR) of reaction center proteins.

All bonded and non bonded parameters, including DFT calculated ESP charges, are available in the supporting material.

Acknowledgments

One of the authors (MM) is pleased to thank Pietro Ballone for enlightening discussions and many suggestions regarding DFT theory and computation.

References

1. Donohoe, R.; Frank, H.; Bocian, D. *Photochem Photobiol* 1988, 48, 531.
2. Palaniappan, V.; Martin, P.; Chynwat, V.; Frank, H.; Bocian, D. *J Am Chem Soc* 1993, 115, 12035.
3. Burie, J.; Boullais, C.; Nonella, M.; Mioskowski, C.; Nabedryk, E.; Breton, J. *J Phys Chem B* 1997, 101, 6607.
4. Marchi, M.; Hutter, J.; Parrinello, M. *J Am Chem Soc* 1996, 118, 7847.
5. Nonella, M.; Brandli, C. *J Phys Chem* 1996, 100, 14549.
6. Ceccarelli, M.; Lutz, M.; Marchi, M. *J Am Chem Soc* 2000, 122, 3532.
7. Car, R.; Parrinello, M. *Phys Rev Lett* 1985, 55, 2471.
8. Röthlisberger, U.; Klein, M. *Chem Phys Lett* 1994, 227, 390.
9. Ballone, P.; Marchi, M. *J Phys Chem A* 1999, 103, 3097.
10. Cornell, W. D.; Cieplak, P.; Bavy, C. I.; Gould, I. R.; Merz, K. M., Jr.; Ferguson, D. M.; Spellmeyer, D. C.; Fox, T.; Caldwell, J. W.; Kollmann, P. *J Am Chem Soc* 1995, 117, 5179.

11. Ceccarelli, M. PhD thesis, Ecole Normale Supérieure, Lyon (2001).
12. Barkigia, K.; Gottfried, D.; Boxer, S.; Fajer, J. *J Am Chem Soc* 1989, 111, 6444.
13. Laasonen, K.; Sprik, M.; Parrinello, M.; Car, R. *J Chem Phys* 1993, 99, 9080.
14. Ballone, P.; Marchi, M.; Branca, C.; Magazù, S. *J Phys Chem B* 2000, 104, 6313.
15. Facelli, J. *J Phys Chem* 1998, 102, 2111.
16. Jones, R. O.; Gunnarson, O. *Rev Mod Phys* 1989, 61, 689; for a review.
17. Becke, A. D. *J Chem Phys* 1986; 84, 4524.
18. Perdew, J. P. *Phys Rev B* 1986, 33, 8822.
19. Hamann, D. R. *Phys Rev B* 1997, 55, 10157.
20. Troullier, N.; Martins, J. L. *Phys Rev B* 1991, 43, 1993.
21. Marx, D.; Hutter, J. *Ab Initio Molecular Dynamics: Theory and Implementation*; John von Neumann Institute for Computing: Jülich, Germany, 2000; vol. 1 of NIC Series, p 301.
22. Pulay, P.; Török, F. *Acta Chim Acad Sci Hung* 1965, 47, 273.
23. Hutter, J. CPMD Program Version 3.0; Tech. Rep.; Max Planck Institut für Festkörperforschung and IBM research: Stuttgart, 1990–1999.
24. Besler, B.; Merz, K.; Kollman, P. *J Comp Chem* 1990, 11, 431.
25. Gelin, B. In *Computer Simulation of Biomolecular Systems*; Gunsteren, W. V.; Weiner, P.; Wilkinson, A., Eds.; ESCOM Science Publishers B.V.: Dordrecht, 1993; p 127, vol. 2.
26. Press, W. H.; Teukolsky, S. A.; Vetterling, W. T.; Flannery, B. P. *Numerical Recipes in Fortran*; Cambridge University Press: Cambridge, UK, 1992; p 644, 2nd ed., chap. 14.
27. Pulay, P.; Fogarasi, G.; Pang, F.; Boggs, J. E. *J Am Chem Soc* 1979, 101, 2550.
28. Andersen, H. C. *J Chem Phys* 1980, 72, 2384.
29. Parrinello, M.; Rahman, A. *J Appl Phys* 1981, 52, 7182.
30. Nose, S. *Mol Phys* 1984, 52, 255.
31. Hoover, W. *Phys Rev A* 1985, 31, 1695.
32. Berendsen, H.; Postma, J.; van Gunsteren, W.; DiNola, A.; Haak, J. *J Chem Phys* 1984, 81, 3684.
33. Marchi, M.; Procacci, P. *J Chem Phys* 1998, 109, 5194.
34. Procacci, P.; Paci, E.; Darden, T.; Marchi, M. *J Comp Chem* 1997, 18, 1848.
35. Darden, T.; York, D.; Pedersen, L. *J Chem Phys* 1993, 98, 10089.
36. Essmann, U.; Perera, L.; Berkowitz, M. L.; Darden, T.; Lee, H.; Pedersen, L. G. *J Chem Phys* 1995, 103, 8577.
37. Marchi, M.; Procacci, P. *J Chem Phys* 1999, 108, 5194.
38. Procacci, P.; Marchi, M. In *Advances in the Computer Simulations of Liquid Crystals*; Zannoni, C.; Pasini, P. Eds.; Kluwer Academic: Dordrecht, The Netherlands, 1999. Proceedings of the NATO-ASI School, Erice 11–21 June 1998; p 333.
39. Lee, S.; Boo, B. *J Phys Chem* 1996, 100, 15073.
40. Wilmshurst, J. *J Mol Spectrosc* 1957, 1, 201.
41. Matzke, P.; Chacón, O.; Andrade, C. *J Mol Spectrosc* 1971, 9, 255.
42. Ryckaert, J. P.; Ciccotti, G.; Berendsen, H. J. C. *J Comput Phys* 1977, 23, 327.
43. Andersen, H. *J Comput Phys* 1983, 52, 24.
44. Robinson, H.; Khan, S. *J Am Chem Soc* 1990, 112, 4728.
45. Nonella, M.; Boullais, C.; Mioskowski, C.; Nabedryk, E.; Breton, J. *J Phys Chem B* 1999, 103, 6363.
46. Ermler, U.; Fritzsche, G.; Buchanan, S.; Michel, H. *Structure* 1994, 2, 925.
47. Burie, J.; Boussac, A.; Boullais, C.; Berger, G.; Mattioli, T.; Mioskowski, C.; Nabedryk, E.; Breton, J. *J Phys Chem* 1995, 99, 4059.
48. Balakrishnan, G.; Mohandas, P.; Umamathy, S. *Spect Acta Part A* 1997, 53, 1553.
49. Smitg, J. V.; Karplus, M. *J Am Chem Soc* 1992, 114, 801.